THE ASTROPHYSICAL JOURNAL, 432:351–366, 1994 September 1


# ATMOSPHERIC PARAMETERS OF FIELD SUBDWARF B STARS

REX A. SAFFER
Space Telescope Science Institute,[1] 3700 San Martin Drive, Baltimore, MD 21218.
saffer@stsci.edu

P. BERGERON
Département de Physique, Université de Montréal, C. P. 6128, Succ. A, Montréal, Québec, Canada H3C 3J7.
bergeron@astro.umontreal.ca

D. KOESTER
Institut für Theoretische Physik und Sternwarte, Olshausenstrasse 40, D-24098 Kiel, Federal Republic of Germany.
supas027@astrophysik.uni-kiel.d400.de

AND

JAMES LIEBERT
Steward Observatory, University of Arizona, Tucson, AZ 85721.
liebert@as.arizona.edu

*Received 1993 December 23; accepted 1994 February 25*

## ABSTRACT

High signal-to-noise ratio optical spectrophotometry of a sample of field subluminous B stars drawn largely from the Palomar Green ultraviolet-excess survey is analyzed with a new grid of model atmospheres and synthetic spectra. The stellar effective temperatures, surface gravities, and photospheric helium abundances are determined simultaneously from a detailed analysis of hydrogen and helium absorption line profiles. The derived temperatures and gravities place the subluminous B stars in the theoretical H-R diagram along and bounded below by theoretical sequences of the zero-age extended horizontal branch, lending strong support to the hypothesis that these stars are composed of helium-burning cores of $\sim 0.5\ M_\odot$ overlain by very thin layers of hydrogen ($\lesssim 0.02\ M_\odot$). Various scenarios for their past evolutionary history are examined in the context of their probable future evolution into white dwarfs of lower than average mass.

*Subject headings:* stars: atmospheres — stars: early-type — stars: horizontal-branch — subdwarfs

## 1. INTRODUCTION

Hot subdwarfs, stars with temperatures exceeding ~25,000 K and surface gravities somewhat higher than main-sequence stars of the same temperature, are thought to be the direct progenitors of the white dwarfs, although they likely comprise only a small fraction of all stars which evolve directly to that state. It is believed that most white dwarfs are formed by low- and intermediate-mass stars evolving toward their final states after the ejection of a planetary nebula at the tip of the asymptotic giant branch. Yet, while the birth rates of planetary nebulae and white dwarfs are estimated to be comparable, the most common objects found in color-selected, magnitude-limited samples such as the Palomar Green (Green, Schmidt, & Liebert 1986) and Kitt Peak Downes surveys (Downes 1986) are the hot subdwarfs. The subdwarf B (sdB) stars have hydrogen-dominated atmospheres, while the subdwarf O (sdO) stars have helium-enriched or helium-dominated atmospheres. An intermediate class (sdOB) also has been identified (Baschek & Norris 1975; Hunger et al. 1981); these stars have effective temperatures and photospheric helium abundances between those of the sdB and sdO stars.

In the past two decades, a number of hypotheses on the origins of the hot subdwarfs have been advanced:

1. Greenstein (1971) and Greenstein & Sargent (1974) first suggested that the sdB stars are the field counterparts of the extreme blue extension of the horizontal branch (extended horizontal branch; EHB) of very metal poor globular clusters. This interpretation is supported by results of the analysis of EHB stars in the globular cluster NGC 6752 by Heber et al. (1986). Some of these stars proved to have atmospheric parameters like those of field sdB and sdOB stars belonging to the disk population, and one star was identified as an sdO, with an effective temperature near 40,000 K. Other globular clusters are known with blue horizontal branches; all have [Fe/H] $\lesssim -1.5$ and are thought to have ages comparable to that of the Galactic halo. Globular clusters with a metal content closer to the solar value and which may be younger than the halo appear to lack blue horizontal branches (see, e.g., Armandroff 1988). On the other hand, recent observations of the ultraviolet energy distributions of more metal-rich globular clusters (Rich, Minniti, & Liebert 1993) have identified ultraviolet excesses at wavelengths shorter than 2000 Å in a handful of clusters. Furthermore, Kałuzny & Udalski (1992) identified seven blue stars in the old, metal-rich open cluster NGC 6791. Similar ultraviolet excesses also have been observed in some metal-rich elliptical galaxies (Burstein et al. 1988). Whether those excesses are due to populations of EHB stars like those in NGC 6752 remains to be determined.

2. The hottest and most luminous subdwarfs might be the descendents of AGB stars whose evolutionary times are longer than the time for dissipation of the nebula. For example, Schönberner & Drilling (1984) and Mendez et al. (1986) discuss sdO stars of low surface gravity which lie in the same region as low-mass post-AGB evolutionary tracks. Horch, Demarque, & Pinsonneault (1993) and Dorman, Rood, & O'Connell (1993) have computed post-EHB evolutionary tracks which, depending on the mass of the hydrogen-rich envelope overlying the helium-burning core, either evolve away from the AGB prior

[1] Operated by the Association of Universities for Research in Astronomy, Inc., for the National Aeronautics and Space Administration.

to the onset of thermal pulsing or fail to ascend the AGB altogether. Some of these tracks also pass through the region of the sdO stars.

3. Close binary evolution could lead to post-RGB phases with effective temperatures and luminosities like hot subdwarfs or to systems that evolve through mergers into hot subdwarfs. Iben & Tutokov (1986a, b) describe calculations of the formation of helium degenerates in which the first mass-loss event occurs after the primary develops a degenerate helium core on the red giant branch, but before it reaches the mass and temperature for core helium burning. Having failed to ignite helium burning, the remnant evolves directly to a low-mass helium (He) degenerate. The secondary subsequently either evolves into a second helium degenerate or into a carbon-oxygen (CO) degenerate. Iben (1990) and Tutukov & Yungelson (1979) have proposed that most subdwarfs could be the product of mergers of He-He or He-CO pairs in these kinds of systems, which release enough gravitational energy in the merger to ignite helium burning. The predicted temperatures and luminosities of the evolving merger products pass through the region of the hot subdwarfs.

In this work, atmospheric parameters are derived for a subsample of the sdB stars defined in the Palomar Green (PG) Survey. Other objects admitted to the sample for analysis include bright and well-studied stars previously classified as sdB, as well as some stars previously misidentified as blue horizontal-branch B (BHB) stars or DA white dwarfs on the basis of low resolution or low signal-to-noise ratio classification spectroscopy. Higher quality spectra of those objects reveal the presence of moderately broadened high Balmer lines extending to $n = 12$, characteristic of sdB stars.

In § 2 the observations are described, and optical spectra of the program objects are presented. In § 3 model spectra of the sdB stars are presented and the procedure used to fit the observations and determine the atmospheric parameters is described, along with an internal and external error analysis. In § 4 the H-R diagram of the sample is discussed, and the implications in terms of the evolutionary history of the sdB stars are examined. The results presented here are compared with those in the literature, including previous determinations of the atmospheric parameters derived from Strömgren colors. A summary is presented in § 5.

## 2. OBSERVATIONS AND REDUCTIONS

Most of the observations described here were obtained at the Steward Observatory Kitt Peak Station with the 2.3 m reflector equipped with the Boller & Chivens Cassegrain spectrograph and UV-flooded TI 800 × 800 CCD. A 600 lines $mm^{-1}$ first-order grating was used behind a 4″.5 × 4′ long slit, which for every observation was rotated to the parallactic angle according to the calculations of Fillipenko (1982). The instrumentation provided wavelength coverage $\lambda\lambda$3650–5200 at a spectral resolution of ~6 Å FWHM. The spectra were extracted from the two-dimensional frames and reduced to linear wavelength and intensity scales using standard reduction packages in the Image Reduction and Analysis Facility (IRAF). Some spectra were obtained at the National Optical Astronomy Observatory's Kitt Peak 2.1 m reflector equipped with the GOLDCAM spectrograph and TI 800 × 800 CCD. This instrumentation provided spectral coverage and resolution similar to that of the 2.3 m instrumentation. A handful of spectra kindly made available by Diana Foss were obtained using the 2.3 m Steward Observatory reflector equipped as described above but using a 1200 lines $mm^{-1}$ first-order grating. The spectral coverage of those observations is from H$\gamma$ through the Balmer jump at 2–3 Å resolution. Spectra of representative program objects are presented in Figure 1, including classical sdB and sdOB stars with $T_{\rm eff} \gtrsim 25{,}000$ K and $\log g \gtrsim 5$, other high-gravity stars with normal or enhanced photospheric helium abundances, apparently normal main-sequence B stars, and very low-gravity stars, possibly in post-EHB or post-AGB evolutionary phases.

The analysis described in § 3 identifies 52 of the 92 program objects as classical sdB stars according to the criteria of Greenstein & Sargent (1974); the effective temperatures lie between about 24,000 K and 42,000 K, the surface gravities exceed $\log g = 5.0$, and the atmospheres are helium-depleted. An additional 15 program objects have surface gravities in excess of $\log g = 5.0$ but have less severely depleted atmospheric helium; some have near-solar or even larger helium abundances. Of the remaining 24 program objects having surface gravities less than $\log g = 5.0$, all but three resemble main-sequence B stars at the intermediate spectral resolution employed here. Alternatively, some of these stars could belong to the blue horizontal branch (BHB). Spectral features which would distinguish between these two classes are not well resolved. For example, at the spectral resolution of the observations shown here, Mg I $\lambda$4481 in main-sequence B stars would be nearly invisible in the red wing of He I $\lambda$4471. The last three objects in the sample show very narrow Balmer absorption features up to $n = 16$, characteristic of giant stars, and their derived surface gravities are well below $\log g = 4.0$.

The 15 helium-strong high-gravity stars have continua and Balmer absorption profiles similar to the classical sdB stars, and show in addition strong, but narrower, He I absorption lines. The hottest of these also show a weak He II $\lambda$4686 absorption feature. Hereafter, both the classical sdB stars and the helium-strong sdB stars shall be referred to as extended horizontal-branch (EHB) stars.

The spectra of four of these low-gravity objects show evidence of reddening. Their spectra show a deficit in their blue and near-UV continua, as would be expected for reddening, instead of the red and near-IR excess in the fluxes expected if red companions were present. Further, the spectra show no apparent absorption features characteristic of low-mass main-sequence stars. Observations at longer wavelengths will be necessary to distinguish between the alternatives.

## 3. ESTIMATION OF STELLAR PARAMETERS

### 3.1. *Line Profile Fitting*

#### 3.1.1. *Synthetic Spectra*

Reliable estimates of the atmospheric parameters $T_{\rm eff}$ and $\log g$ can be obtained by simultaneously fitting line profiles of the members of the Balmer series with appropriate model spectra. For example, Bergeron, Saffer, & Liebert (1992) obtained atmospheric parameters for 129 DA white dwarfs using this technique. Pure hydrogen model atmospheres were calculated in LTE and incorporated hydrogen-line blanketing. Theoretical spectra were calculated using the occupation probability formalism of Hummer & Mihalas (1988), as described in Bergeron et al. (1992). Computed in a similar manner, the model grid used here encompasses the following ranges of atmospheric parameters: $20{,}000 < T_{\rm eff} < 40{,}000$ K, $4.0 < \log g < 6.0$, and $0.0 < y \equiv N({\rm He})/N({\rm H}) < 0.1$. The grid spac-

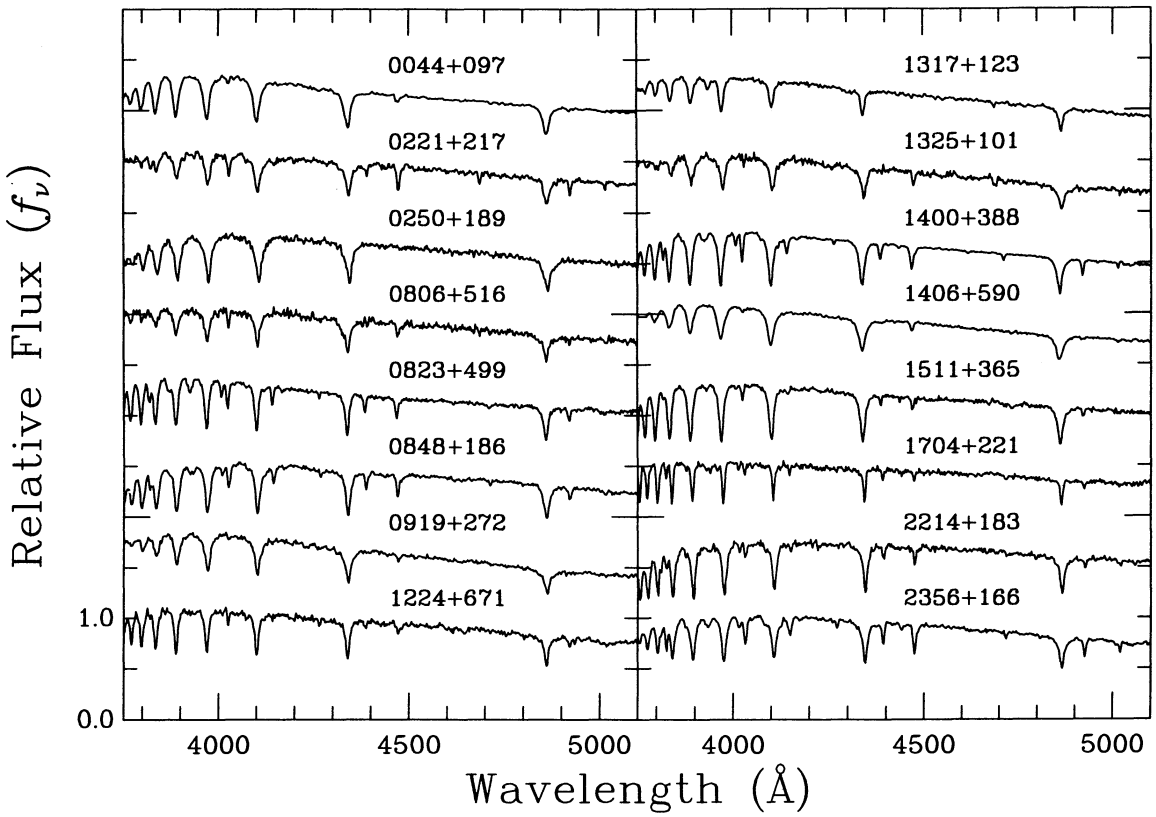


FIG. 1.—Representative observed spectra of subluminous B star candidates

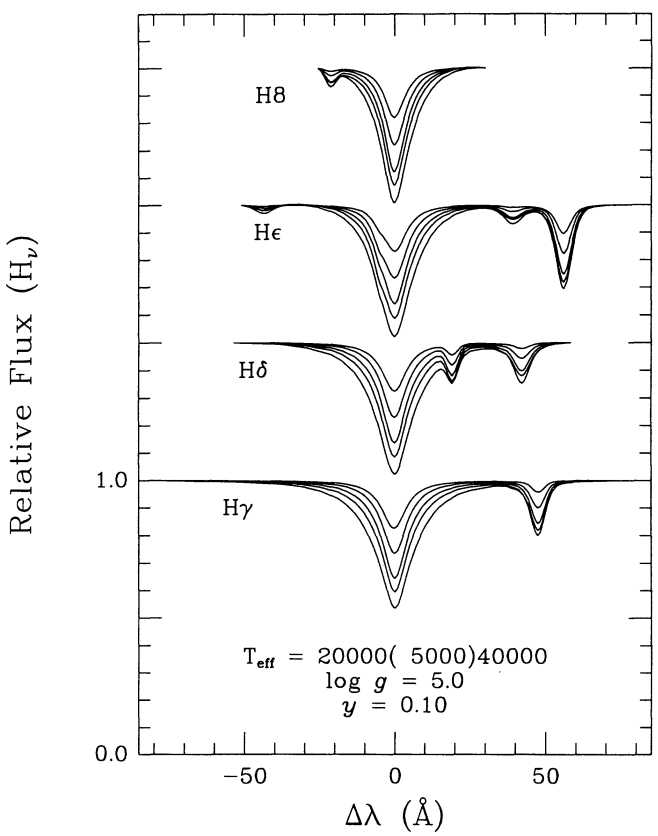


FIG. 2a

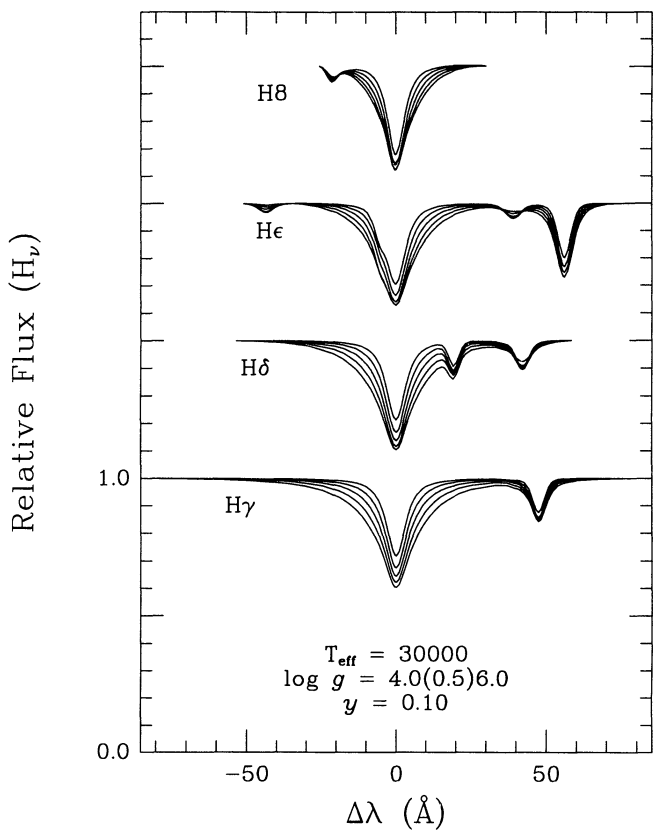


FIG. 2b

FIG. 2.—(*a*) Normalized theoretical spectra showing the effects of effective temperature variations at fixed surface gravity on hydrogen and helium line profiles. For each Balmer line, the uppermost profile has the highest temperature. (*b*) As for (*a*), but for line profile variations with changes in surface gravity at fixed effective temperature. For each Balmer line, the uppermost profile has the lowest surface gravity.

ings are 5000 K, 0.5 dex, and 0.03 by number, respectively. In Figures 2*a* and 2*b*, the effects of variations in effective temperature and surface gravity on the theoretical Balmer and helium line profiles are shown.

It is known that for the hottest stars the details of both absorption- and emission-line profiles are strongly affected by non-LTE processes (see, e.g., Kudritzki & Hummer 1990 for a review of quantitative spectroscopy of hot stars). However, Wesemael et al. (1980) find good agreement for continuum fluxes in comparisons of LTE and non-LTE calculations at subdwarf surface gravities, although an overpopulation of the $n = 2$ level strengthens the Balmer line cores. Another comparison of LTE and non-LTE atmospheres and model spectra in the subdwarf B regime (S. Vennes, private communication) shows that the higher Balmer members have line profiles that differ from those calculated in LTE only in the core, and that the differences are small and not easily detected at the spectral resolution of the observations employed in this work.

Other factors which might affect the shapes of the line profiles are the presence of rapid rotation or of strong magnetic fields. However, either of these processes affects the line profile shapes in a fundamentally different manner than do variations in the line profiles with variations in either effective temperature or surface gravity. Convolution of theoretical line profiles with rotational broadening functions shows that for rotation velocities in excess of some 100 km $s^{-1}$, the line profiles are perturbed to the extent that a satisfactory fit to the observed spectra cannot be found for any choice of atmospheric parameters (assuming zero rotation). Magnetic fields are first manifested as a flattening of the line cores as the Zeeman components split in magnetic fields of order $10^6$ G, with Zeeman triplets become noticeably visible at field strengths in excess of $10^7$ G. At very high field strengths, the spectra cease to resemble at all the zero-field spectra as the quadratic Zeeman effect adds to the magnetic broadening of the line profiles. In either case the result is the same as for significant rotation; the spectra cannot be satisfactorily fit by zero-field model line profiles for any choice of atmospheric parameters. In the sample analyzed here, only one star fails to be well fitted (PG 2218+051, discussed subsequently), and for the rest of the stars in the sample the conclusion is that these stars neither rotate rapidly nor do they have strong magnetic fields in the line-forming regions of the atmosphere.

#### 3.1.2. *Least-Squares Fitting Procedure*

In the fitting procedure used by Bergeron et al. (1992), the observed and theoretical Balmer line profiles are normalized to a linear continuum, and the atmospheric parameters $T_{\rm eff}$ and log $g$ are determined with least-squares fitting techniques. Here the technique is extended to three dimensions, and the effective temperature, surface gravity, and helium abundance are determined simultaneously by fitting theoretical spectra to a single optical spectrum of the program object.

The nonlinear least-squares algorithm (Press et al. 1986) used to estimate the atmospheric parameters must be provided with good initial estimates of the parameters. Inspection of the $\chi^2$ surface shows that the location of the global minimum agrees well with parameter estimates based on the appearance of the spectra, and for all objects, the fitting algorithm converges rapidly to a solution for which all lines are fitted well. A detailed discussion of the fitting procedure is given by Saffer (1991).

Selected model fits to spectra of confirmed EHB stars are shown in Figure 3. The fits are excellent; indeed, for many of the fits it is difficult to distinguish the model spectra from the data. With the exception of one star (PG 2218+051, discussed below), it was possible to achieve repeatable, rapidly converging solutions for a wide range of reasonable initial conditions. Figure 4 shows fits for nonsubdwarf members of the sample. Some 26% of all stars selected as sdB candidates based on the PG spectral classifications fall into the nonsubdwarf category. The low signal-to-noise ratios characteristic of follow-up classification spectroscopy of large, color-selected surveys make it difficult to resolve line profile variations that discriminate changes in surface gravity, especially if only the lower, less gravity-sensitive Balmer lines are analyzed. It is important to include the higher Balmer lines in classification spectra of hot, subluminous stars if clear separation of luminosity classes is desired at intermediate spectral resolution.

One star, PG 2218+051, could not be well fitted for any choice of atmospheric parameters. Classified sdOA on the basis of its broad, strong Balmer absorption and strong He I absorption, the star has anomalously broad and somewhat flat-bottomed He II $\lambda$4686 and He I line profiles. It is possible that this is due to its high derived helium abundance of $N$(He)/$N$(H) = 0.148, well outside the limits of the model atmosphere grid. However, a second star with high derived helium abundance and similar effective temperature and surface gravity [PG 2128+096, $N$(He)/$N$(H) = 0.156] was well fitted by the synthetic spectrum grid. High-resolution observations of the H$\alpha$ line core are planned to investigate whether the star is rapidly rotating, as well as spectropolarimetric observations to detect possible magnetic fields of order 1 MG or less. An average of the atmospheric parameters of fits analyzing various combinations of low and high Balmer lines has been adopted for this work. These estimates should be considered uncertain pending further analyses.

### 3.2. *Atmospheric Parameter Error Estimation*

#### 3.2.1. *Internal Error Estimation*

In the least-squares fitting procedure, the spectra first are fitted with the weights set to unity. After convergence, the weights are calculated by computing the rms deviations of the data from the best-fit model, averaged over short segments of the spectrum. A second, weighted fit is then performed, and the resulting parameter estimates are adopted for the object. The weights then are propagated into the covariance matrix of the fit, from which the single-measurement internal error estimates are derived (cf. Press et al. 1986). A more detailed discussion of the dependence of internal error estimates on variations in the flux calibration and extinction correction is given by Saffer (1991), where the modes of the $T_{\rm eff}$, log $g$, and $N$(He)/$N$(H) error distributions take values of 500 K, 0.12 dex, and 0.003 by number, respectively.

The derived atmospheric parameters are more uncertain in some regimes. At low temperature and surface gravity, metals in the atmosphere are not depeleted by diffusion and are blended with hydrogen and helium lines, and line cores are affected to some extent by departures from LTE. At the spectral resolution of the observations, weaker lines useful as luminosity indicators are not well detected. Some estimates extrapolated beyond the model grid parameter space are highly uncertain. Happily, most estimates lie inside the grid, or nearly so. More accurate determinations of atmospheric parameters for the lower gravity stars await an analysis of

1994ApJ...432..351S

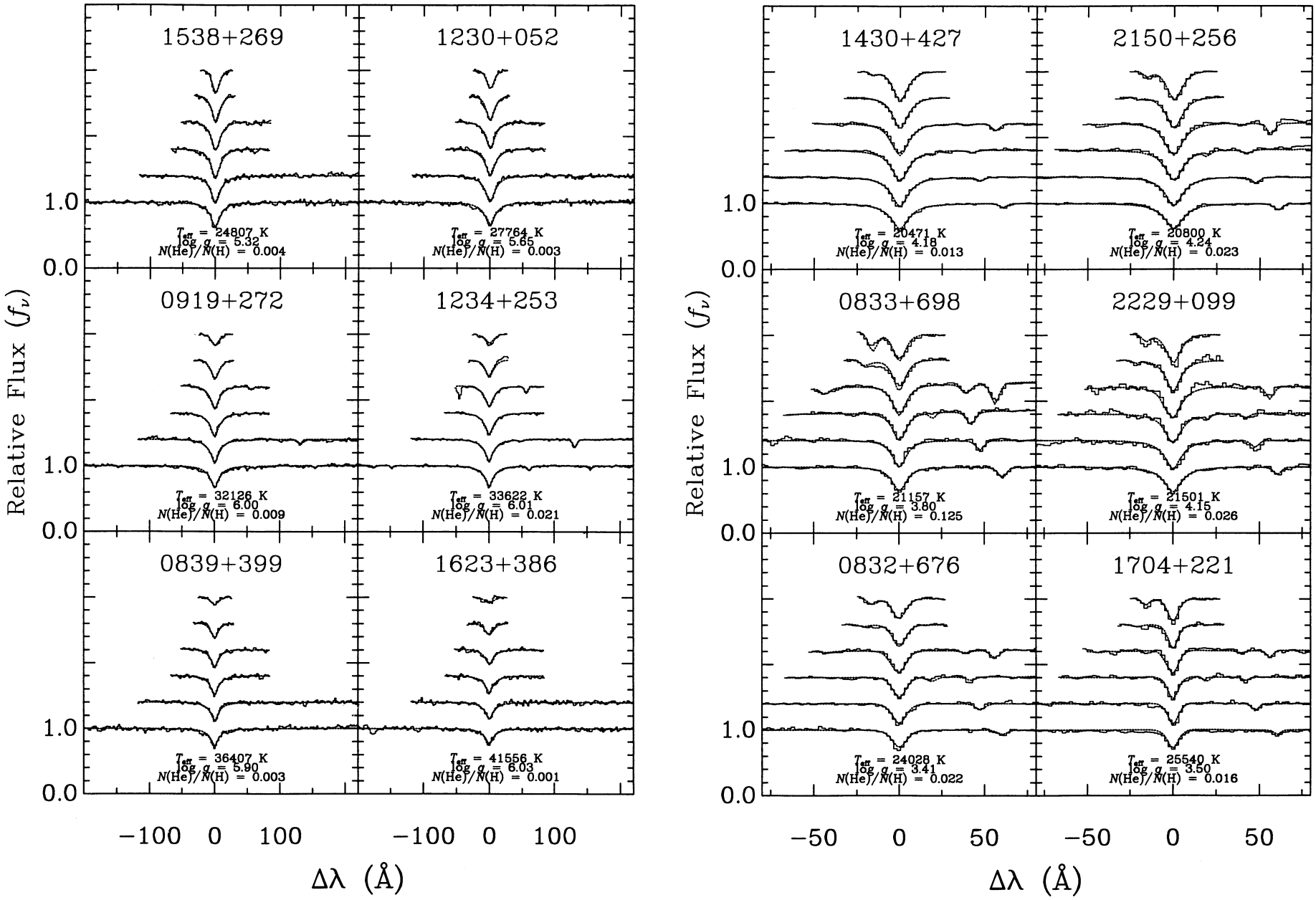


FIG. 3.—Model fits (*dotted lines*) to observed spectra (*solid lines*) of confirmed EHB stars
FIG. 4.—Model fits (*dotted lines*) to observed spectra (*solid lines*) of misclassified non-EHB stars. The horizontal scale has been expanded to show better detail in the narrower line profiles.

higher resolution spectra with appropriate models. Still, the analysis performed here serves to cull low-gravity stars from the confirmed EHB sample and gives a rough estimate of their luminosities.

#### 3.2.2. *External Error Estimation*

Another independent estimate of the derived parameter uncertainties is possible through repeated measurements of any given object. While no program object in the sample was observed often enough to make a meaningful estimate of its parameter uncertainties, one of the flux standards, Feige 34, was observed many times throughout the course of the project. Feige 34 is a hot, atmospheric helium–enriched subdwarf O star, which nonetheless has a hydrogen-dominated atmosphere. Several independent spectra of Feige 34 obtained on five different nights separated by at least several weeks were analyzed in the same manner as the program objects. The rms deviations of estimated effective temperature and surface gravity about the means of the distributions were in excellent agreement with the internal error estimates. No other significant sources of random error appear to contribute to the parameter uncertainties. The question of whether systematic errors result in inaccurate or biased estimates is addressed below by comparisons of the spectrosopic parameter estimates with those derived by other methods of analysis of well-studied subluminous B stars.

#### 3.2.3. *Variation with Atmospheric Seeing*

Another source of possible error in the derived atmospheric parameters is variations in the atmospheric seeing. The slit width used for all observations was 4".5, and combined with other sources of instrumental broadening, this always gave well-exposed, unblended comparison lamp emission lines with 8 Å FWHM. The seeing almost never was that bad, with 1"–2" seeing more common. This corresponds more closely to 4–6 Å spectral resolution. In general, if spectra are analyzed with model grids convolved with a resolution element that has a FWHM that is too small (large) compared with the observations, the model line cores will be too deep (shallow), and effective temperatures and surface gravities that are too high (low) will be required to fit any given spectrum, at least for temperatures characteristic of EHB and main-sequence B stars. For every fit to observed spectra, the adopted parameter estimates correspond to the resolution giving the smallest value of $\chi^2$ for the model fit.

#### 3.2.4. *Final Adopted Error Estimates*

After taking all sources of random and systematic error into consideration, it is useful to define characteristic individual measurement errors for each atmospheric parameter estimate, which may then be compared against the observed distributions of the sample. For example, the morphology of the distribution of EHB stars in the $T_{\rm eff}$–log $g$ diagram may be used to confirm or rule out certain theories of their evolution, if it can be shown that the measurement errors are small enough to provide discriminatory power. For $T_{\rm eff}$, log $g$, and $N$(He)/$N$(H), those characteristic 1 $\sigma$ errors are estimated to be 1000 K, 0.15 dex, and 0.01 by number, respectively.

### 3.3. *Best-Fit Atmospheric Parameter Estimates*

In this work, stars were selected for observation and analysis if the PG spectral classification was given as sd, sdB, sdB–O, or sdOA. Three other classes of objects also appear in the sample:

1. Of the DA white dwarfs selected from the catalog of McCook & Sion (1987) for the sample of Bergeron et al. (1992), 10 stars proved upon inspection of high signal-to-noise ratio blue spectra to have high Balmer lines extending at least to $n = 12$. The analysis performed here shows that nine of those stars have effective temperatures and surface gravities characteristic of subdwarf B stars, and the tenth has the temperature and gravity of a main-sequence B star.

2. From a sample of blue horizontal-branch B star (BHB) candidates observed by Diana Foss, five stars proved to be subdwarf B stars.

3. Five other known subdwarf B stars and one main-sequence B3 V standard not inluded in the PG survey were chosen for observation and analysis. The subdwarfs were included because they have previously been analyzed in other investigations, and comparisons with other determinations of the atmospheric parameters of subdwarf B stars are useful. The main-sequence star 16 Peg was observed for the purpose of comparison with the nonsubdwarf contaminators of the sample.

Table 1 presents the best-fit derived atmopheric effective temperatures, surface gravities, and helium abundances for 68 confirmed EHB stars. The columns labeled "$B_{\rm PG}$" and "PG Sp" give the $B$ magnitude and spectral classification listed in the PG Catalog. Table 2 presents derived parameters for 24 nonsubdwarf stars in the sample having surface gravities less than log $g = 5.0$. These objects comprise 26% of the sample.

## 4. EHB STARS IN THE H-R DIAGRAM

### 4.1. *Effective Temperatures and Surface Gravities*

The derived effective temperatures and surface gravities for the entire sample of 92 sdB candidates are displayed in Figure 5. The open symbols distinguish ranges of photospheric helium abundance, and connected filled symbols denote the zero-age helium-burning main sequence (HeMS), zero-age extended horizontal branch (ZAEHB), zero-age horizontal branch (ZAHB), and zero-age hydrogen-burning main sequence (HMS) as indicated in the legend: diamonds—HeMS, Paczyński (1971); circles—HeMS and ZAEHB, Caloi (1972, 1989); triangles—ZAHB and ZAEHB, Sweigart (1987); and HMS, Allen (1973). The HeMS is labeled with the stellar mass in solar units. The solid lines rising from the ZAEHB represent post-EHB evolutionary tracks taken from Caloi (1989), labeled with the total stellar mass. The error bars show the adopted (1 $\sigma$) measurement errors of 1000 K and 0.15 dex. The stars represented in the figure can be divided into three broad classes:

1. Classical sdB and sdOB stars having effective temperatures between 24,000 and 42,000 K and surface gravities exceeding log $g = 5.0$, and having helium-deficient photospheres [$N$(He)/$N$(H) $\lesssim 0.02$].

2. Stars with temperatures and surface gravities characteristic of classical sdB and sdOB stars but having normal or even enhanced helium abundances compared to the solar value. These stars tend to have the highest effective temperatures and lie near the helium main sequence, as well as near some of the relatively cool and higher gravity helium-rich sdO stars.

3. Lower gravity main-sequence B and blue horizontal-branch stars having photospheric helium abundances ranging from normal to mildly depleted compared to the solar value.

At temperatures approaching 15,000 K, the theoretical horizontal branch and main sequence begin to overlap, making

TABLE 1

PG CONFIRMED EHB ATMOSPHERIC PARAMETERS

| Object | Name | $B_{PG}$ | $T_3$ (K) | log $g$ | $y$ | PG Sp | Remark |
|---|---|---|---|---|---|---|---|
| 0044+097 | HD 4539 | ... | 27.0 | 5.46 | 0.005 | NPG sdB | ... |
| 0101+039 | Feige 11 | 10.98 | 28.4 | 5.63 | 0.005 | sdB | ... |
| 0111+177 | ... | 15.85 | 30.9 | 5.57 | 0.013 | DA3 | Visual double |
| 0112+142 | ... | 14.70 | 38.5 | 5.82 | 0.004 | sdB | ... |
| 0212+230 | ... | 15.36 | 26.4 | 5.80 | 0.004 | sdB–O | ... |
| 0221+217 | ... | 15.62 | 33.6 | 5.87 | 0.118 | DA2 | ... |
| 0242+132 | ... | 11.78 | 31.2 | 5.65 | 0.023 | sdOA | ... |
| 0250+189 | ... | 13.65 | 26.1 | 5.81 | 0.001 | sdB | ... |
| 0319+054 | ... | 14.92 | 30.5 | 5.61 | 0.019 | DA3 | ... |
| 0322+114 | ... | 15.26 | 26.6 | 5.72 | 0.002 | sdB | ... |
| 0342+026 | ... | 11.07 | 26.2 | 5.67 | 0.004 | sdB | ... |
| 0349+094 | ... | 15.69 | 25.4 | 5.74 | 0.002 | sdB | ... |
| 0749+658 | ... | 10.75 | 24.6 | 5.54 | 0.004 | sdB–O | ... |
| 0806+516 | ... | 15.03 | 34.9 | 6.13 | 0.027 | sdB | ... |
| 0816+313 | Ton 313 | 15.64 | 32.4 | 5.99 | 0.010 | sdB | ... |
| 0823+465 | ... | 14.55 | 29.9 | 5.75 | 0.002 | sdB | ... |
| 0839+399 | K345–30 | 13.87 | 36.1 | 5.91 | 0.002 | sd | Visual double |
| 0856+121 | ... | 13.06 | 26.4 | 5.73 | 0.001 | sdB | ... |
| 0909+275 | ... | 10.74 | 35.4 | 6.02 | 0.121 | sdOA | ... |
| 0910+621 | ... | 15.54 | 28.8 | 5.57 | 0.002 | DA3 | ... |
| 0918+029 | ... | 12.49 | 31.7 | 6.03 | 0.008 | sdB–O | ... |
| 0919+272 | Ton 13 | 11.95 | 31.9 | 5.97 | 0.011 | sdB | ... |
| 0920+296 | Ton 14 | 14.58 | 31.3 | 6.15 | 0.052 | sdOA | CB 5 |
| 0933+383 | K347–17 | 15.28 | 27.7 | 5.55 | 0.006 | DA2 | ... |
| 0940+171 | ... | 16.13 | 27.9 | 5.69 | 0.007 | BHB | ... |
| 0941+280 | Ton 22 | 12.46 | 29.0 | 5.58 | 0.001 | BHB | ... |
| 0947+639 | ... | 14.78 | 30.5 | 5.60 | 0.001 | DA 3 | ... |
| 1012+007 | ... | 14.82 | 32.2 | 5.99 | 0.014 | sdB | ... |
| 1101+249 | Feige 36 | 12.98 | 29.6 | 5.82 | 0.013 | sd | ... |
| 1114+072 | Feige 38 | 12.96 | 29.8 | 5.81 | 0.006 | sdB | ... |
| 1154−070 | ... | 13.52 | 28.2 | 5.58 | 0.005 | sd | ... |
| 1230+052 | ... | 12.45 | 28.3 | 5.72 | 0.001 | sdB | ... |
| 1232−136 | ... | 13.43 | 29.0 | 5.69 | 0.034 | sdOA | ... |
| 1233+426 | Feige 65 | 11.90 | 26.5 | 5.60 | 0.005 | sdB | ... |
| 1234+253 | Feige 66 | ... | 33.4 | 6.20 | 0.017 | NPG sdB | ... |
| 1236+479 | Ton 96 | 15.26 | 27.9 | 5.47 | 0.004 | DA2 | ... |
| 1255+547 | ... | 13.40 | 33.4 | 5.81 | 0.027 | sdOA | ... |
| 1256+278 | HZ 38 | 14.14 | 34.4 | 5.93 | 0.118 | sdOA | ... |
| 1303−114 | ... | 13.53 | 31.9 | 5.97 | 0.003 | sd | ... |
| 1313+132 | Feige 75 | 14.48 | 25.6 | 5.41 | 0.001 | BHB | ... |
| 1325+101 | ... | 13.29 | 34.5 | 6.11 | 0.021 | sdB–O | ... |
| 1343−101 | ... | 11.99 | 28.9 | 5.65 | 0.001 | sdB–O | ... |
| 1432+158 | ... | 13.66 | 26.9 | 5.75 | 0.008 | sdB | ... |
| 1433+240 | Ton 209 | 10.71 | 29.6 | 5.57 | 0.000 | sdB | ... |
| 1438−029 | ... | 13.82 | 27.7 | 5.50 | 0.005 | BHB | ... |
| 1442+342 | ... | 14.40 | 29.9 | 5.80 | 0.006 | sd | ... |
| 1538+269 | Ton 245 | 13.18 | 25.2 | 5.30 | 0.003 | DA2 | ... |
| 1559+533 | ... | 14.38 | 30.8 | 5.85 | 0.007 | sdOA | ... |
| 1613+426 | KUV | 14.39 | 34.4 | 5.97 | 0.022 | sdOA | ... |
| 1619+522 | ... | 12.84 | 32.3 | 5.98 | 0.011 | sdB | ... |
| 1623+386 | KUV | 15.43 | 41.6 | 6.10 | 0.008 | sd | Visual double |
| 1631−039 | HD 149382 | ... | 34.2 | 5.89 | 0.026 | NPG sdB | ... |
| 1636+216 | ... | 14.61 | 34.3 | 5.76 | 0.018 | BHB | ... |
| 1643+209 | ... | 14.82 | 30.2 | 5.62 | 0.023 | sdB | ... |
| 1708+409 | ... | 15.09 | 28.5 | 5.33 | 0.006 | sdB | ... |
| 1710+490 | ... | 12.06 | 29.9 | 5.74 | 0.006 | sdB | ... |
| 1716+426 | ... | 13.69 | 27.4 | 5.47 | 0.003 | sdB | ... |
| 1758+364 | KUV | ... | 32.1 | 5.91 | 0.015 | NPG sdB | ... |
| 2059+013 | ... | 13.95 | 32.4 | 5.80 | 0.020 | sdB | ... |
| 2110+127 | ... | 13.56 | 33.7 | 5.33 | 0.004 | sdB | Composite |

FIG. 1—*Continued*

| Object | Name | $B_{PG}$ | $T_3$ (K) | log $g$ | $y$ | PG Sp | Remark |
|---|---|---|---|---|---|---|---|
| 2128+096 | ... | 14.25 | 39.4 | 5.87 | 0.156 | sdOA | ... |
| 2128+112 | ... | 15.73 | 33.5 | 5.58 | 0.001 | DA2 | ... |
| 2204+034 | ... | 13.44 | 31.4 | 5.96 | 0.018 | sdB–O | ... |
| 2218+051 | ... | 15.30 | 36.5 | 6.20 | 0.148 | sdOA | Anomalous |
| 2313−021 | Feige 108 | ... | 34.5 | 6.01 | 0.001 | NPG sdB | ... |
| 2317+046 | PB 5333 | 11.38 | 37.9 | 5.81 | 0.002 | sdB | $y$ uncertain |
| 2345+318 | ... | 14.37 | 27.5 | 5.70 | 0.006 | sdB | ... |
| 2349+001 | PB 5562 | 12.02 | 29.3 | 5.77 | 0.000 | sdB | ... |

these stars difficult to distinguish from each other at the intermediate spectral resolution of the observations.

The confirmed EHB stars cluster in a well-defined sequence lying parallel to theoretical sequences of the zero-age extended horizontal branch (ZAEHB; Caloi 1972, 1989) and zero-age horizontal branch (ZAHB; Sweigart 1987). For all stars with log $g \gtrsim 5.0$, every star resides within a sloping band with vertical cross section $\sim 0.5$ dex and bounded below by the ZAEHB sequence with mass $\sim 0.5\ M_\odot$. The theoretical sequences are parameterized by $q = M_c/M_*$, the ratio of the helium-burning core mass to total mass. For the $0.5\ M_\odot$ sequence shown in Figure 5, $q = 0.92$ and 0.98 at $T_{\rm eff} = 20{,}000$ and 26,000 K, respectively. For $q \gtrsim 0.96$, corresponding to an envelope mass $M_e \lesssim 0.02\ M_\odot$, it is not possible to sustain hydrogen shell burning as it is for cooler horizontal-branch stars, which derive a significant fraction of their luminiosty from hydrogen shell burning. For the same reason, those stars are unable to ascend the asymptotic giant branch after the end of the core helium-burning phase. The subsequent evolution of an EHB star in the H-R diagram should resemble that of a pure helium star of the same mass.

Grouped in the third class with the lower gravity stars, a distribution of stars with surface gravities between the main sequence and the EHB sequence is evident, with the separation from those two sequences becoming quite pronounced at effective temperatures between 25,000 and 35,000 K. The EHB evolutionary tracks of Caloi (1989) suggest that the intermediate sequence might be composed of post-EHB stars. For EHB tracks with an initial helium-burning core mass of $0.5\ M_\odot$ and envelope masses of 0.003, 0.005, and $0.01\ M_\odot$, calculations of the phases immediately after core helium exhaustion show a gradual rise in luminosity over a period of some $2 \times 10^7$ yr. The ratio of this timescale to the core helium-burning timescale of $\sim 1.3 \times 10^8$ yr predicts that for the 68 confirmed EHB stars one would expect $\sim 10$ stars in post-EHB configurations. The observed intermediate distribution in Figure 5 is consistent with these predictions. Following the gradual rise to the upper boundary of the post-EHB area, the stars rapidly evolve to high temperature and luminosity in a phase lasting only some $10^5$ yr, after which they join the white dwarf cooling sequence. Thus, the region in the H-R diagram hotter than $\sim 40{,}000$ K and with surface gravity lower than log $g \sim 5.0$ would not be expected to be populated, and no stars in the sample are found to lie there. A similar behavior in more massive horizontal-

TABLE 2

PG NONSUBDWARF ATMOSPHERIC PARAMETERS

| Object | Name | $B_{PG}$ | $T_3(K)$ | log $g$ | $y$ | PG Sp | Remark |
|---|---|---|---|---|---|---|---|
| 0229+064 | ... | 11.50 | 22.0 | 4.65 | 0.137 | sdOA | Ca II "K" |
| 0823+499 | ... | 11.04 | 20.1 | 3.95 | 0.133 | sdOA | Ca II "K" |
| 0832+675 | ... | 14.23 | 29.2 | 3.99 | 0.015 | sdOA | ... |
| 0833+698 | ... | 13.27 | 21.6 | 3.83 | 0.120 | sdOA | Ca II "K" |
| 0848+186 | ... | 13.09 | 21.5 | 4.63 | 0.106 | sdOA | Ca II "K" |
| 0855+293 | CB 29 | 10.34 | 22.2 | 4.06 | 0.076 | BHB | ... |
| 1208+224 | ... | 14.33 | 26.0 | 3.55 | 0.007 | sdOA | Giant |
| 1223+058 | ... | 15.99 | 20.0 | 4.51 | 0.007 | sdB | Ca II "K" |
| 1224+671 | ... | 11.64 | 29.3 | 4.86 | 0.012 | sdB–O | ... |
| 1257+276 | HZ 47 | 15.37 | 19.6 | 4.42 | 0.025 | sdOA | ... |
| 1317+123 | Feige 80 | 9.01 | 32.8 | 4.83 | 0.006 | sdO | Ca II "K" |
| 1323−085 | ... | 12.63 | 27.0 | 3.70 | 0.009 | sdB–O | Giant; composite? |
| 1400+388 | PB 1207 | 12.05 | 21.6 | 4.75 | 0.113 | sdOA | Ca II "K" |
| 1430+427 | ... | 14.55 | 20.1 | 4.12 | 0.012 | DA2 | ... |
| 1607+173 | KUV | 10.24 | 27.6 | 4.92 | 0.153 | sdOA | Ca II "K" |
| 1704+221 | ... | 11.77 | 26.2 | 3.72 | 0.015 | sdB–O | Giant; composite? |
| 2135+044 | ... | 13.97 | 32.1 | 4.79 | 0.016 | DA2 | ... |
| 2150+256 | 16 Peg | ... | 20.5 | 4.20 | 0.025 | NPG B3V | Standard star |
| 2214+183 | ... | 13.57 | 18.6 | 4.26 | 0.023 | sd | Composite? |
| 2219+093 | ... | 9.41 | 29.7 | 4.60 | 0.021 | sdO | Ca II "K" |
| 2229+099 | ... | 12.61 | 18.1 | 3.90 | 0.085 | sd | Ca II "K" |
| 2301+259 | ... | 12.16 | 21.3 | 4.21 | 0.013 | sdB | ... |
| 2345+241 | ... | 11.58 | 22.4 | 4.07 | 0.021 | sdB–O | Ca II "K" |
| 2356+166 | ... | 13.92 | 23.8 | 4.70 | 0.148 | sdB–O | Ca II "K" |

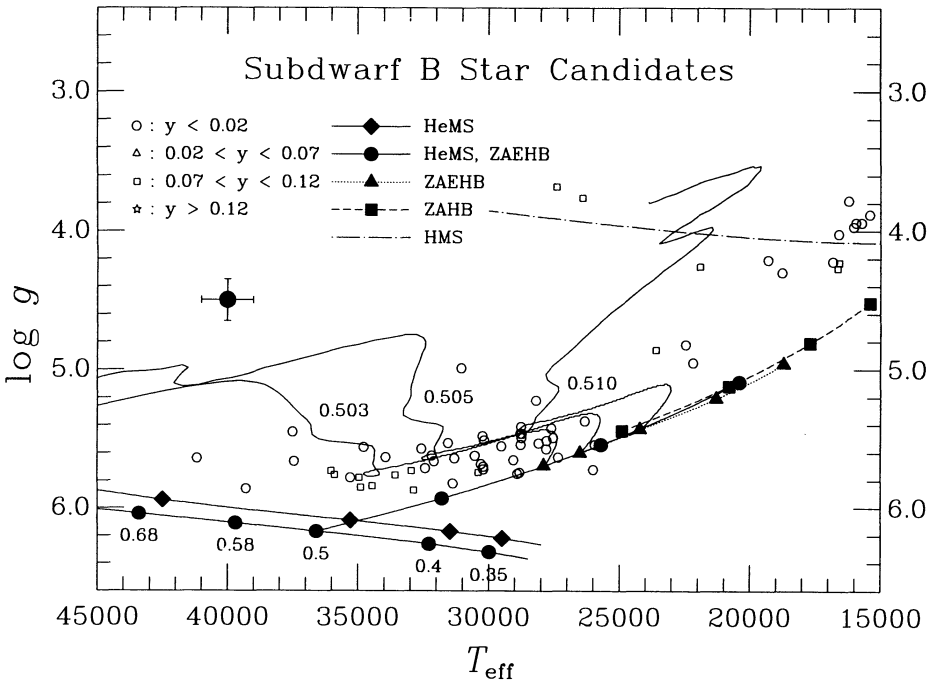


FIG. 5.—Derived effective temperatures and surface gravities for 92 sdB candidates (*open symbols*). See the text for details.

branch stars after the exhaustion of central helium has been demonstrated by Strom et al. (1970) for the so-called supra–horizontal-branch stars in the globular cluster M3.

### 4.2. *The Field Horizontal-Branch Gap*

The EHB sequence is well populated at surface gravities exceeding log $g = 5.0$ and effective temperatures exceeding 25,000 K. Near $T_{\rm eff} = 24{,}500$ K, the sequence ends abruptly. This cutoff is in good agreement with the boundary defined by the blue edge of the second Newell gap in the cumulative distribution of the density of field BHB stars versus the reddening-free Strömgren index $[u-b]$ (Newell & Graham 1976). That study demonstrated the existence of two gaps, centered on $[u-b] \sim 0.95$ and $[u-b] \sim 0.25$, with widths that, according to the temperature calibration of Philip & Newell (1975), correspond to effective temperature intervals of 12,800–13,300 K and 20,000–23,000 K, respectively. It should be noted that the observed cutoff is not related to the color selection criterion $(U-B) < -0.46$ imposed on objects detected and selected for follow-up spectroscopic classification in the PG survey. At effective temperatures exceeding 20,000 K, all stars having surface gravities exceeding those of main-sequence stars have $(U-B) \lesssim -0.8$, so that even with the large uncertainty of 0.38 mag in the $(U-B)$ colors of the PG catalog, hot B stars are not selected against in the survey. Only for stars as late as B5–B7 (15,000–13,000 K) would the selection effect begin to become important. Even at those temperatures only the stars with the lowest surface gravities would be selected against.

Unambiguous evidence exists for similar gaps in the blue horizontal branches of four metal-poor globular clusters: NGC 6752 (Cannon 1981), NGC 288 (Buonanno et al. 1984), M15 (Buonanno, Corsi, & Fusi Pecci 1985), and $\omega$ Cen (Da Costa, Norris, & Villumsen 1986, hereafter DCNV). However, DCNV report that the midpoints of the gaps in those clusters have effective temperatures of 20,000 K, 12,900 K, 10,000 K, and 16,200 K, respectively. There appears to be no correlation between mean cluster metallicity and gap position. The cluster gaps might be identified with one of the Newell gaps for field BHB stars in NGC 6752 and NGC 288, but the field and cluster gaps cannot be demonstrated to be related. The very existence of such gaps, either in the field or in clusters, is troublesome in terms of current stellar evolution theory. Evolutionary models do not predict gaps if the various physical processes which might affect HB morphology, such as age, mass loss, envelope helium and heavy metal abundances, and stellar rotation, are continuously distributed (cf. Rood & Crocker 1985). Bimodal cyanogen distributions are seen in the giant branch stars in some clusters having gaps in their blue horizontal branches, and CNO abundance is one candidate for the long-sought "second parameter" influencing cluster HB morphology (Norris et al. 1981; Norris 1981; Smith & Norris 1982, 1983). But DCNV find no evidence for a bimodal CN distribution in the giant branch of $\omega$ Cen, which demonstrably possesses a well-defined BHB gap.

For the most part, the gaps in globular cluster blue horizontal branches are not completely unpopulated by stars. Rood & Crocker (1985) and Crocker, Rood, & O'Connell (1986, 1988) have demonstrated bimodality in a number of globular cluster blue horizontal branches. They suggest the gaps are not places that stars have evolved away from, or where stars are forbidden, but rather are the underpopulated regions lying between the bimodal distributions of BHB stars. The mass distribution of BHB stars in M15 is best explained under this hypothesis by a pair of Gaussian distributions with overlapping tails. The high mass (red) distribution is centered on 0.67 $M_\odot$ with $\sigma \sim 0.025$ $M_\odot$, and the low-mass (blue) distribution is centered on 0.59 $M_\odot$ with $\sigma \sim 0.01$ $M_\odot$ (Rood & Crocker 1985).

The dearth of objects on the 0.5 $M_\odot$ ZAHB tracks in Figure 5 at effective temperatures cooler than 24,000 K might be due

to the omission of PG objects classified as blue horizontal-branch stars from the sample analyzed here. Another possibility is that the cutoff is a selection effect due to the subdwarf classification criteria of the PG survey: weak hydrogen-lined candidates were rejected if absorption was detected at Ca II "K." That criterion might have led to rejection of cooler EHB stars at surface gravities somewhat less than $\log g = 5.0$ and effective temperatures between 15,000 K and 25,000 K. However, while it is true that none of the 68 confirmed EHB stars show detectable Ca II "K" there are a dozen examples in the nonsubdwarf contaminators that were classified as PG subdwarfs and that show detectable Ca II "K" absorption with equivalent widths $\sim 1$ Å. These stars are identified in the "Remarks" column of Table 2. No star falls on the theoretical EHB tracks in Figure 5. Only one star has an effective temperature between 23,000 K and 24,500 K, and its surface gravity of $\log g = 4.70$ separates it cleanly from the EHB stars. Richard Green has provided the authors with the classification spectra of several hundred stars rejected from the subdwarf category because of the clear detection of Ca II "K" absorption. Careful inspection of these spectra identified only a handful of stars that have weak hydrogen lines, and at the same time show weak Ca II "K" while lacking altogether any hint of a "G" band or Mg I "$b$" absorption. Thus it seems quite unlikely that the low-temperature EHB cutoff is due to this selection effect.

The cutoff in the EHB distribution in Figure 5 also coincides with the position along the model evolutionary sequences where the overlying hydrogen-rich envelope has a mass $\sim 0.02$ $M_\odot$ ($q \sim 0.96$), the mass below which hydrogen shell-burning cannot be sustained. Further investigations of the atmospheric parameters of field blue horizontal-branch stars are badly needed to determine the extent and nature of gaps in the field Population I horizontal and extended horizontal branches. Unfortunately, such analyses are complicated greatly by the confluence of the hydrogen-burning main sequence and the blue horizontal branch at cooler effective temperatures and are beyond the scope of this work. Observations at higher spectral resolution and analyses using appropriate model grids will be required to extend the current investigation to cooler temperatures.

At the hot end, the EHB sequence is populated by hydrogen-rich stars at temperatures as high as 40,000 K, overlapping to some extent with low-luminosity sdO stars having helium enriched atmospheres. There are no stars found to have surface gravities higher than those of the theoretical helium main sequences (HeMS) of Paczyński (1971, *upper track*) and Caloi (1989, *lower track*) shown in Figure 5. This is further evidence in favor of the EHB interpretation of the subdwarf B stars, since the HeMS is the limiting case of the mass of the overlying hydrogen-rich envelope of a core helium-burning star going to zero.

### 4.3. *Photospheric Helium Abundances*

The helium abundances of all the program objects are plotted against effective temperature in Figure 6, where the three broad subdivisions of the sample noted previously are distinguished by different symbols. The open circles represent classical sdB stars, having helium abundances $y \lesssim 0.02$, an arbitrary standard, but one consistent with the notion of depleted atmospheric helium at sdB surface gravities. High gravity stars with $y > 0.02$ are identified by open boxes and labeled "He-strong," or at least closer to the solar value compared to classical sdB stars, and low gravity stars are identified by open triangles. The figure shows a clear boundary in effective temperature at some 30,000 K, below which all high-gravity objects have helium-depleted atmospheres. A trend to higher helium abundance at higher temperatures is evident, and the distribution becomes modestly bifurcated at the highest effective temperatures ($T_{\rm eff} \gtrsim 35{,}000$ K), where approximately equal numbers of stars have either very high or very low helium abundance. The model grid is bounded above by $y = 0.10$, and for the highest derived helium abundances all that can be said is that they are significantly in excess of the solar value. An extension of the model grid to higher helium abundances is needed to determine the abundances more accurately for the most helium-rich component of the sample.

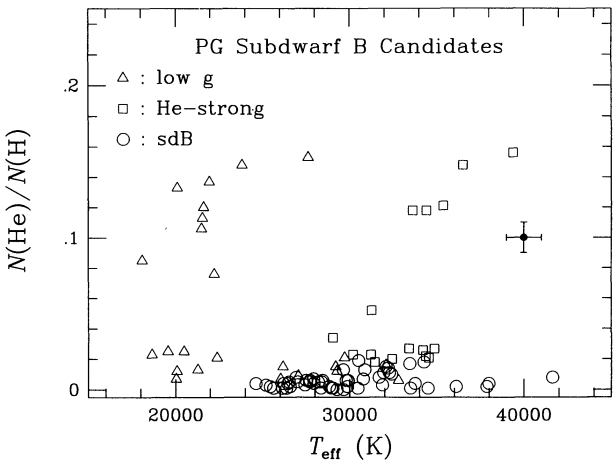


FIG. 6.—Photospheric helium abundance vs. effective temperature

Many of the helium-strong stars have PG spectral classifications of sdB–O or sdOA, i.e., those stars of apparently higher gravity having moderate to strong He I absorption lines. As discussed subsequently, these helium abundance patterns are difficult to reconcile with time-dependent diffusion calculations, which predict depletion of all helium from the photosphere on very short timescales over the whole range of characteristic EHB effective temperatures.

### 4.4. *Comparisons with Other Analyses*

All previous analyses of EHB stars have been carried out in a similar manner: First, the effective temperature is estimated from an analysis of the ultraviolet energy distribution or from intermediate- or narrow-band photometry. The effective temperature then is held fixed while a Balmer line profile, typically H$\gamma$, is analyzed for the surface gravity. Finally, the equivalent width or detailed shape of the line profile of a strong helium line, like He I $\lambda$4471, gives an estimate of the helium abundance. The last two steps may have to be iterated at higher helium abundances. Unfortunately, with the exception of the recent works of Moehler et al. (1990b) and Moehler, Heber, & de Boer (1990a, hereafter MHdB), with which comparisons will be discussed in the next section, most previous analyses of stars analyzed in this work either have quite uncertain surface gravity determinations or lack them altogether. The only other extensive body of accurate surface gravity determinations (see, e.g., Heber et al. 1984, Groth, Kudritzki, & Heber 1985, and Heber 1986) is for southern hemisphere stars for which there is little overlap with this sample.

While most of the program objects selected for analysis in

TABLE 3

COMPARISONS WITH PREVIOUS DETERMINATIONS

| Object | $T_3$ (K) (This Work) | $T_3$ (K) (Other) | log $g$ (This Work) | log $g$ (Other) | Reference | Primary Temperature Diagnostic[a] |
|---|---|---|---|---|---|---|
| HD 4539 | 27.0 | 25.0 | 5.46 | 5.4 | 1 | 1 |
| | | 26.0 | | | 2 | 2 |
| | | 24.8 | | 5.4 | 3 | 2, 3 |
| Feige 11 | 28.4 | 28.8 | 5.63 | | 2 | 2 |
| | | 26.9 | | 5.5 | 3 | 2, 3 |
| PG 0342+026 | 26.2 | 21.8 | 5.67 | 5.0 | 4 | 3 |
| Feige 36 | 29.6 | 29.2 | | | 2 | 2 |
| Feige 38 | 29.8 | 30.2 | | | 2 | 2 |
| Feige 65 | 26.5 | 26.2 | 5.60 | 5.3 | 5 | 4 |
| Feige 66 | 33.4 | 36.0 | 6.20 | 6.0 | 6 | 5 |
| | | 35.0 | | | 2 | 2 |
| | | 35.7 | | | 7 | 3 |
| Feige 75 | 25.6 | 25.3 | | | 2 | 2 |
| Ton 209 | 29.6 | 29.3 | | | 2 | 2 |
| Ton 245 | 25.2 | 24.0 | | | 2 | 2 |
| HD 149382 | 34.2 | 40.0 | 5.89 | 5.8 | 8 | 1 |
| | | 35.0 | | 5.5 | 9 | 6 |
| UV 1758+364 | 32.1 | 32.5 | 5.91 | 5.25 | 10 | 1, 3 |
| | | 31.8 | | 5.6 | 5 | 4 |
| Feige 108 | 34.5 | 35.0 | | | 2 | 2 |

REFERENCES.—(1) Baschek et al. 1972; (2) Bergeron et al. 1984; (3) Heber & Langhans 1986; (4) Lamontagne et al. 1987; (5) Lamontagne et al. 1985; (6) Baschek et al. 1982a; (7) Wesemael et al. 1985; (8) Baschek & Norris 1975; (9) Baschek et al. 1982b; (10) Giddings & Dworetsky 1978.

[a] PRIMARY TEMPERATURE DIAGNOSTIC.—(1) Line wing shapes; (2) Strömgren colors; (3) UV continuum; (4) Composite UV and optical continuum; (5) Ionization equilibria; (6) H and He equivalent widths.

this work were chosen from the Palomar Green survey, the compilation of Kilkenny, Heber, & Drilling (1987) provides data on some 200 spectroscopically classified hot subdwarfs, 100 of which have been analyzed for effective temperature and surface gravity. Of the EHB component in this catalog, 13 stars having 19 independent effective temperature estimates were selected for observation and analysis here, and of these, seven stars have nine independent surface gravity estimates. These exclude the temperature and gravity estimates of MHdB, which will be discussed subsequently.

Table 3 summarizes these previous analyses, and the table and Figures 7*a* and 7*b* show comparisons of those results with the results of the analysis performed in this work. There is excellent agreement between the spectroscopic temperature estimates derived here and estimates derived by other groups using the methods specified next to the various symbols in the legend. It is important to note that, save for the discrepant points in the lower left-hand and upper right-hand corners of the figure, the agreement is excellent without regard to the method of estimation of the effective temperature. The first significantly discrepant point (for PG 0342+026) is taken from Lamontagne, Wesemael, & Fontaine (1987), in which the authors warn of potential uncertainties in having substituted the LWP camera of the *IUE Observatory* for the LWR camera used in previous investigations. The second discrepant point (for HD 149382) was taken from Baschek & Norris (1975). An

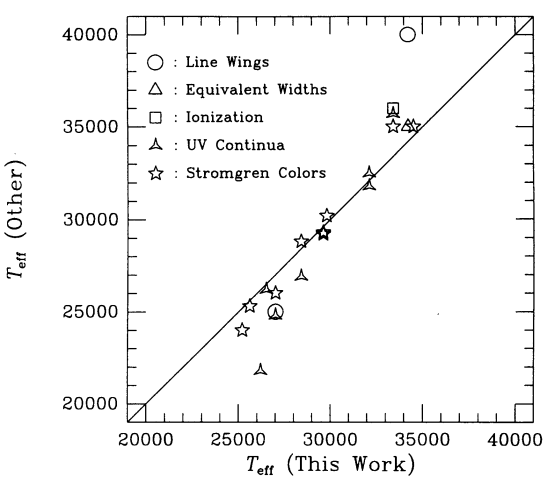


FIG. 7*a*

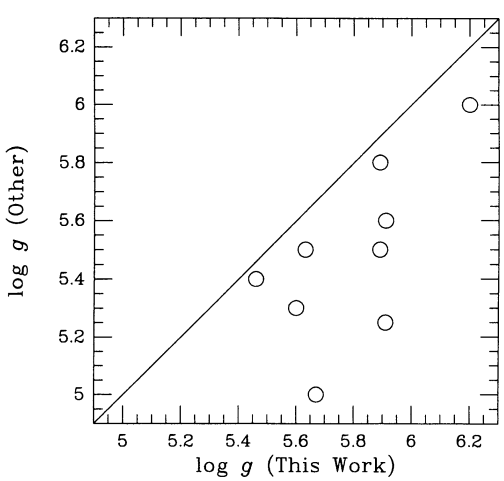


FIG. 7*b*

FIG. 7.—(a) Comparison with effective temperature estimates in the literature. (*b*) Comparison with surface gravity estimates in the literature.

improved determination for the same star was given by Baschek et al. (1982b), who attributed the difference with the previous result to a much improved model atmosphere analysis.

The agreement for surface gravity estimates is not as good as for the effective temperatures, with other estimates having slightly lower derived values. The most discrepant points are for the same star having the most discrepant temperature estimate, and for an early, admittedly uncertain estimate of the surface gravity of UV 1758+364 by Giddings & Dworetsky (1978). There is no compelling explanation for the systematic shift of the remaining seven points.

### 4.5. *Estimates from Spectroscopy versus Colors*

A more extensive check of the internal consistency of the temperature and gravity estimates in this work is possible using Strömgren colors from Wesemael et al. (1992), in which all PG sdB and sdOA stars with photographic $B$ magnitudes brighter than 14.6 were observed. By calibrating a color index versus effective temperature scale with the model grid used to analyze the spectra, it is possible to compare derived effective temperatures for a considerable portion of the sample using that Strömgren photometry.

The Strömgren colors $(b - y)$ and $(u - b)$ were calculated for the $y = 0$ model grid, using the sensitivity functions and the calibration of Olson (1974). For each effective temperature and surface gravity, the reddening-free index $[u - b] = (u - b) - 1.56(b - y)$ was calculated, and following Bergeron et al. (1984), for each effective temperature an average value of $[u - b]$ was calculated from the two values of $[u - b]$ for log $g = 5.0$ and 6.0. For 51 stars in the sample having measured Strömgren colors, the resulting $[u - b]$ versus $T_{\rm eff}$ relation then was interpolated for the stellar effective temperatures. Those derived effective temperatures were compared against effective temperatures derived from the same data, but using the $[u - b]$ versus $T_{\rm eff}$ relation of Bergeron et al. (1984). The correlation is excellent over the common range of $T_{\rm eff}$.

Figure 8 shows a comparison of effective temperatures derived in the three-parameter fits versus the effective temperatures derived from Strömgren colors, for 45 of the 51 stars in the spectroscopic sample having measured Strömgren colors. For the remaining six stars, the color temperature estimates are wildly discrepant, and these have been excluded from the comparison. Two of these stars have blue $(b - y)$ colors between $-0.075$ and $-0.15$ mag and with $(u - b)$ colors that are significantly more negative than the bulk of the stars with the comparable $(b - y)$ colors. Due to the steep color index versus effective temperature relation at high temperatures, their positions in the two-color diagram above the 45,000 K thoeretical reddening line correspond to derived effective temperatures as high as 60,000 K. The accompanying photometric errors are of order 0.05 mag, and observational error could be responsible. The presence of unresolved red companions also could account for the discrepancy by making $(b - y)$ more positive, although the PG Catalog does not identify the stars as composite, nor is there any record in the observing logs of the objects having been resolved on the acquisition camera monitor. The three very low gravity objects in the sample have color temperatures between 6000 K and 12,000 K lower than their spectroscopic temperatures. It is inappropriate to have analyzed them with the temperature relation calibrated with high-gravity model spectra, and they also have been excluded from the comparison. The last star, which has a color temperature some 10,000 K less than the spectroscopic temperature, shows a dramatic downturn in flux in the blue part of its spectrum, evidence of reddening or the presence of a companion.

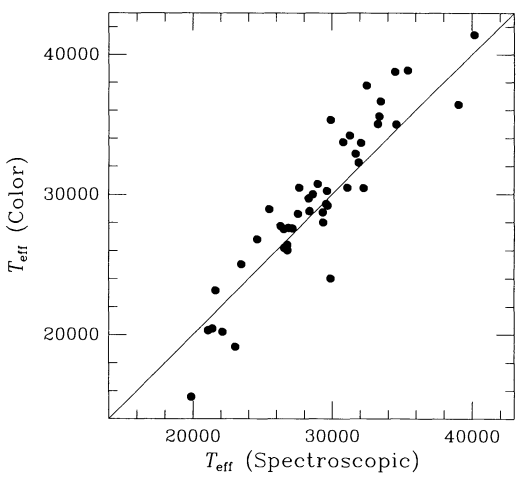


FIG. 8.—Internal comparison of effective temperatures derived from spectroscopy and colors.

Figure 8 shows that for the remaining 45 stars, the agreement is good, considering the uncertainty of the color-$T_{\rm eff}$ calibration. There is a mild systematic trend at high $T_{\rm eff}$, but this is not significant given the relatively large errors in the color temperature estimates. The rms deviation of the points about the diagonal line is $\langle \Delta T_{\rm eff} \rangle_{\rm rms} = 2400$ K, only some 8% at $T_{\rm eff} = 30{,}000$ K. The most discrepant stars have a range of helium abundances, so that differences in the model atmosphere helium abundances do not appear to have significantly affected the estimates. The discrepancy may not be significant, since the $[u - b]$ versus $T_{\rm eff}$ relation is very steep at high $T_{\rm eff}$, and small differences in the measured and theoretical colors correspond to large differences in $T_{\rm eff}$. Non-LTE effects might become significant at high $T_{\rm eff}$, but as previously noted, Wesmael et al. (1980) found no significant difference in continuum fluxes in the EHB regime.

### 4.6. *Further Temperature and Gravity Comparisons*

Moehler et al. (1990b) and MHdB have presented spectra and atmospheric analyses for 92 stars selected from the PG Catalog, including 37 confirmed EHB stars. In those analyses, effective temperature estimates were derived from ultraviolet energy distributions or optical photometry. The surface gravities then were derived from an analysis of the H$\gamma$ profile made while holding $T_{\rm eff}$ fixed. In the sample presented here, there is overlap with the MHdB sample only for 19 stars, and of those only 13 were analyzed by MHdB for the atmospheric parameters. Moehler et al. (1990b) report Strömgren photometry and show spectra for the remaining six stars, but their effective temperature and surface gravity estimates are not reported.

Comparisons of derived effective temperatures for the stars in common with MHdB are shown in Figure 9*a*. There is a significant rms systematic difference of 2750 K in the color temperature scales of this work and of MHdB in the range 25,000–35,000 K. The cooler MHdB estimates were derived either from their own photometry or that of Fontaine et al. (1987). For stars common to both photometric samples the reported colors are in good agreement, and its seems likely that

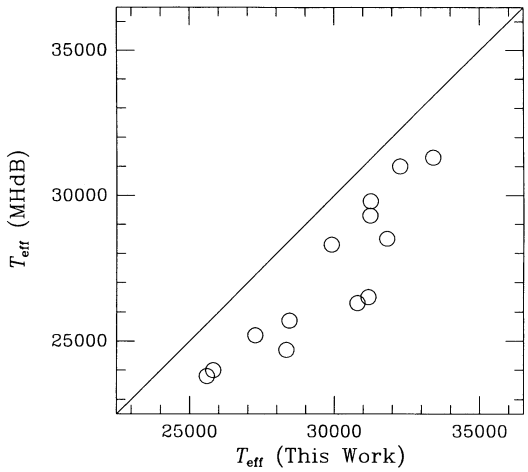


FIG. 9a

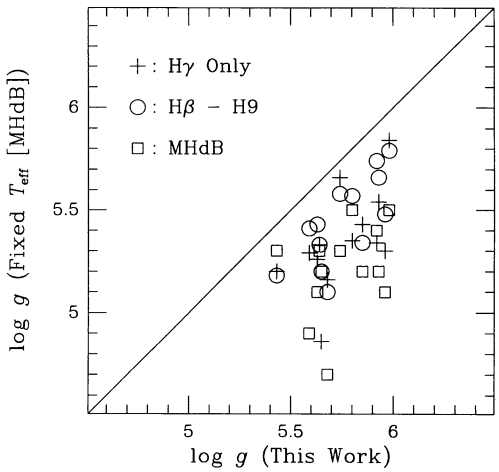


FIG. 9b

FIG. 9.—(*a*) Comparison of derived effective temperatures with the sample of Moehler et al. (1990b) and MHdB. (*b*) Comparison of derived surface gravities of the same sample. The values denoted by plus and cross symbols were derived by holding the effective temperature fixed at the value cited by MHdB and analyzing the indicated Balmer lines for the surface gravity.

the discrepancy lies in the $[u - b]$ versus $T_{\rm eff}$ calibration. Indeed, MHdB used a calibration based on the models of Lester, Gray, & Kurucz (1986) with solar composition and log $g = 4.5$–$5.0$. The difference between their calibration and the one used here can fully account for the discrepancy in the derived color temperatures. As shown previously, the color temperature estimates derived from the Olson (1974) calibration of the $y = 0$ model grid used here and the spectroscopic temperature estimates derived from the three-parameter fits agree closely between 25,000 and 35,000 K (Fig. 8*a*). If the Lester et al. (1986) calibration had been used, that comparison would have shown a systematic offset similar to that seen in Figure 9*a*.

To compare surface gravities derived from the lower resolution spectra analyzed here, effective temperatures were held fixed at the values cited by MHdB, and gravities were determined by fitting first Hγ (following MHdB), then all available Balmer lines in each spectrum (Fig. 9*b*). The resulting gravity estimates are significantly lower than the spectroscopic estimates, as expected considering the significantly lower estimated temperatures of MHdB, and they are not improved by fitting all available Balmer lines. The rms difference in gravity is 0.55 dex, a very large discrepancy in terms of the derived stellar luminosity, and to a lesser extent the derived distances. If the theoretical EHB tracks corresponding to a core mass of 0.5 $M_\odot$ shown in Figure 5 are displaced upward in surface gravity by 0.55 dex, the intersection of those tracks with the helium main-sequence tracks implies a significant increase in the derived EHB core mass to as much as 0.7 $M_\odot$. This is uncomfortably high if the sdB stars are identified with the EHB, and if their immediate progenitors are red giant branch stars, which for an old disk population might be expected to be producing large numbers of 0.45–0.5 $M_\odot$ cores at helium ignition.

When the effective temperatures were held fixed at the MHdB values, it proved possible to fit Hγ and Hδ satisfactorily for all the stars in common with MHdB, even when the higher Balmer lines were obviously poorly fitted. The difference need only be as large as 2000–3000 K to induce quite large surface gravity differences of up to 0.8 dex compared to the estimates derived in three-parameter fits. The spectra analyzed by MHdB covered λλ4000–5000 at 2.5 Å resolution, with the red wing of Hβ and continuum not detected. The line is unsuitable for fitting because the continuum redward of the line cannot be established accurately, leaving only Hγ and Hδ available for analysis. Spectral coverage λλ3750–4750 makes available for analysis Hγ–H9 as gravity-sensitive lines while still covering the strong He II line at λ4686, a useful diagnostic at higher effective temperature.

### 4.7. *Luminosity Evolution and Core Mass Dispersion*

Greenstein & Sargent (1974) first identified the field sdB stars with the EHB, and pointed out that for core helium-burning stars, log $(g\theta^4)$ scales with log $(L/L_\odot)$ and is constant for a given core mass, with $\theta = 5040\ {\rm K}/T_{\rm eff}$. If the uncertainties in the derived atmospheric parameters were small enough, any existing structure in the EHB luminosity distribution might be resolved, e.g., the luminosity evolution during the $\sim 10^8$ yr core helium-burning lifetime. Alternatively, the dispersion due to a distribution of core masses significantly larger than that due to luminosity evolution might be resolved.

In Figure 10*a*, log $(g\theta^4)$ is plotted against $\theta$ for 68 confirmed classical sdB and helium-strong sdB stars with derived surface gravities in excess of log $g = 5.0$. The 1 σ error bars shown in the figure were computed from the individual internal errors of the model fits, and the unweighted mean 1 σ uncertainty of the individual measurements is about 0.16 in log $(g\theta^4)$. The apparent trend to higher luminosity with increasing effective temperature is not significant. A weighted average gives a best-fit constant value of log $(g\theta^4) = 2.64$, of the same order as the value of 2.38 determined by Greenstein & Sargent (1974). In Figure 10*b*, the histogram shows the number distribution of log $(g\theta^4)$ for the stars of Figure 10*a* and the accompanying mean 1 σ error. The distribution is broad; in fact, its FWHM of $\sim 0.4$ in log $(g\theta^4)$ is only marginally larger than the FWHM of a normal distribution having a 1 σ standard deviation of 0.16. Hence most, if not all, of the width of the distribution is due to observational error. There is no significant structure to suggest that any underlying luminosity evolution has been resolved, which if present would result in a skew to higher density at smaller values of log $(g\theta^4)$ (i.e., higher luminosity.)

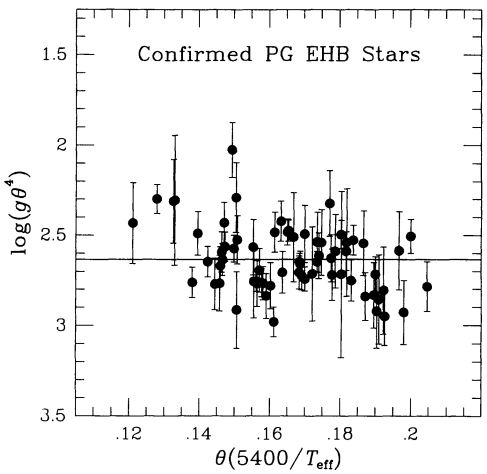


FIG. 10*a*

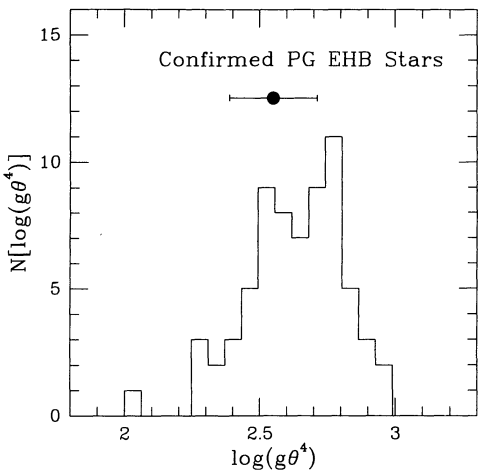


FIG. 10*b*

FIG. 10.—(*a*) For 68 confirmed EHB stars, log ($g\theta^4$) is constant. (*b*) Number distribution of log ($g\theta^4$). The core mass distribution is unresolved.

Neither does the distribution support a conservative 1 $\sigma$ dispersion in core mass larger than about 0.04 $M_\odot$.

The narrow distribution of core masses about the 0.5 $M_\odot$ EHB tracks in Figure 5 constrains the range of initial masses of prospective EHB progenitors if they are red giant branch (RGB) stars which lose the bulk of their hydrogen-rich envelope at the tip of the RGB. Calculations by Sweigart, Greggio, & Renzini (1989, 1990, hereafter together SGR) have explored the evolution of the RGB as a function of the initial mass of the turnoff stars in a stellar population. For low-mass stars, there are profound differences in the morphology of the RGB, the luminosity at its tip, and the core mass at helium ignition compared to intermediate-mass stars. The intermediate-mass stars ignite helium quietly under nondegenerate conditions shortly after reaching the RGB and have a short-lived and low-luminosity RGB phase. The low-mass stars ignite helium violently under degenerate conditions and have a more luminous and long-lived RGB phase. The SGR evolutionary sequences span a range of initial masses from 1.4 to 3.4 $M_\odot$. The SGR "RGB phase transition," marked by a rapid increase in the luminosity, extent, and lifetime of the RGB phase as the turnoff stars begin to ignite helium in a degenerate core, takes place over a narrow range of initial masses between 2.0 and 2.8 $M_\odot$, depending on the initial helium and metal mass fractions $Y$ and $Z$.

Of more interest in the context of the apparently narrow range of EHB core masses inferred here is the value of the core mass at helium ignition at the tip of the RGB. For initial masses below $\sim$2.0 $M_\odot$, irrespective of the initial metal abundances, the core mass at helium ignition converges to a value between 0.46 and 0.48 $M_\odot$ for initial helium mass fractions of 0.30 and 0.20, respectively. Sweigart & Gross (1978) found the core mass to be $\sim$0.47 $M_\odot$ for an initial mass of 0.8 $M_\odot$ and for $Y = 0.30$ and $Z = 0.01$, values appropriate for old disk stars. For $Z = 0.01$, and $Y = 0.20$ and 0.30, the core mass at ignition reaches an absolute minimum of $\sim$0.33 $M_\odot$ for initial masses of $\sim$2.7 and $\sim$2.3 $M_\odot$, respectively. For initial masses larger than these, the core mass increases monotonically. Thus, if disk RGB stars are the immediate progenitors of the field EHB stars, their initial masses are constrained to be $\lesssim 2$ $M_\odot$. For initial masses between 4 and 5 $M_\odot$, the core masses at helium ignition also would be near 0.5 $M_\odot$ (Castellani, Chieffi, & Straniero 1990), but there are too few of those more massive stars to account for the bulk of the EHB stars. The kinematics of EHB stars (Saffer 1991) also suggest that their progenitors are older, less massive disk stars.

Several previous determinations of the masses of evolved stars and stellar remnants also have narrow derived mass distributions. Weidemann & Koester (1984) found for DA white dwarfs with effective temperatures between 8000 K and 15,000 K a distribution with a narrow peak, an extended high-mass tail, and a sharp low-mass cutoff. Bergeron et al. (1992) found a similar distribution for DA white dwarfs hotter than 15,000 K, although their analysis, with its significantly better mass resolution, identified a separate population of very low-mass white dwarfs that presumably derive from close binary evolution (see also Liebert, Bergeron, & Saffer 1991). If this group of stars is excluded from the comparison, however, all previously determined white dwarf mass distributions have remarkably similar shapes with the salient feature being a very narrow central peak. Mendez (1987) found for 21 Galactic planetary nebula central stars a peaked mass distribution with 11 stars in the central two 0.05 $M_\odot$ bins. Jacoby (1989) and Ciardullo et al. (1989) found it necessary to assume a planetary central star mass distribution centered on 0.61 $M_\odot$ and having a Gaussian dispersion of only 0.02 $M_\odot$ in order to fit the luminosity function of the brightest planetary nebulae in the Local Group. However, there could be a selection effect, the "guillotine" effect, which selects against the most (least) massive planetary central stars because the evolutionary timescales for those stars are too short (long) for the nebulae to become bright enough for long enough to be detected. Still, neither very high- nor very low-mass central stars are known to exist in abundance.

### 4.8. *Astrophysical Implications*

The morphology of the EHB sequence shown in Figure 5 strongly supports the core helium-burning interpretation of the EHB and is inconsistent with the hypothesis that the majority of these stars are in post-AGB evolutionary states. If the interpretation of the sequence as one of continuously decreasing envelope mass is correct, and if the narrow width of the distribution correctly implies a narrow range of core masses, evolution from RGB progenitors might account for the majority of the field EHB stars. The kinematics of the sample (Saffer 1991) strongly indicate membership in the old disk population, and upon completing RGB evolution such a popu-

lation would contribute large numbers of helium-burning stars with core masses near 0.5 $M_\odot$ to the field horizontal branch population. Only a small fraction of all RGB stars would have to lose the bulk of their hydrogen-rich envelopes to account for the observed birthrate of field EHB stars, assuming core helium-burning lifetimes. It is difficult, however, to reconcile this scenario with the observed characteristics of horizontal branches in disk globular clusters. Those clusters have metallicites much closer to the solar value than those in globular clusters with [Fe/H] $\lesssim -1.5$. On the basis of studies of both more metal-rich globular clusters and old galacitc clusters, these stars would be expected to have very red core helium-burning horizontal branches and very sparse or nonexistent blue horizontal branches and extended horizontal branches. This is believed to be the case for horizontal branch stars in known old disk clusters like M67 and NGC 188.

Alternate hypotheses for the origins of the EHB stars predict a larger mass dispersion for a core helium-burning sequence than is observed. Iben & Tutukov (1986a) have calculated the evolution of a close binary system that first undergoes Roche lobe overflow when the primary has become a giant with a degenerate helium core with a mass of 0.3 $M_\odot$. When the envelope around this degenerate core is lost, the binary detaches, and its subsequent evolution is driven by the contraction of the inert helium core. There are three stages of evolution with luminosities reaching or exceeding those of the EHB stars. The first and longest lived of these stages lasts for about $5 \times 10^6$ yr, evolving at a nearly constant luminosity dominated by residual hydrogen burning at the base of the envelope. The other two stages last for only $3 \times 10^5$ yr and $5 \times 10^3$ yr, respectively. More massive remnants would evolve even more rapidly than this example. If one takes the longest lived phase for the 0.3 $M_\odot$ core and uses the sdB space density of Downes (1986; $2 \times 10^{-6}$ pc$^{-3}$), the resulting birthrate is $dn/dt \sim 2 \times 10^{-12}$ yr$^{-1}$ pc$^{-3}$, or about the same as the birthrate of all white dwarfs. This is too high if all EHB stars evolve directly to the white dwarf cooling sequence, since the vast majority of white dwarfs are believed to evolve directly from the central stars of planetary nebulae.

This hypothesis predicts that there would be a spectrum of remnant core masses, depending on the initial mass of the primary, mass ratio, and orbital separation in the way described by Iben & Tutukov (1986b). This picture is inconsistent with the narrow width of the EHB distribution in surface gravity. At $T_{\rm eff} = 25{,}000$ K, the 0.3 $M_\odot$ core would have log $g \sim 4.6$, with the higher mass cores having even lower surface gravity. Only for very low mass cores would the evolutionary tracks overlap the observed EHB surface gravities. Those calculations also predict that the bulk of EHB stars should be radial velocity variables with amplitudes of many tens, or even hundreds, of km s$^{-1}$. Saffer (1991) has made multiple measurements of radial velocities of nearly 50 of the stars in the sample presented here. Only five of these stars have radial velocities measured at different epochs which differ by more than 3 standard deviations ($\sigma \sim 15$–$30$ km s$^{-1}$), inconsistent with this close binary hypothesis for the origin of the majority of EHB stars.

In related scenarios, Iben (1990) calculates the evolution of close binary systems leading to mergers of He-He and CO-He degenerate cores. These mergers can result in core helium-burning stars with masses ranging from 0.3 $M_\odot$ to 0.7 $M_\odot$. Such a dispersion in core mass would result in a smearing of the distribution in the theoretical H-R diagram in the direction parallel to the HeMS, inconsistent with the observed distribution. However, as the somewhat hotter sdO stars exhibit a considerably larger range of surface gravities than the EHB stars analyzed here (see, e.g., Hunger et al. 1981, Schönberner & Drilling 1984, and Groth et al. 1985), it is possible that some fraction of those stars might have evolved from both types of mergers, especially given the hydrogen-poor composition expected from prior common envelope evolution.

The distribution of photospheric helium abundances also helps to test the various origin hypotheses. In Figure 6, the derived photospheric helium abundances for all program objects are plotted against effective temperature. Michaud et al. (1989) have made detailed non-LTE calculations of radiative acceleration on helium in model atmospheres appropriate to sdOB stars. For $N(\mathrm{He})/N(\mathrm{H}) = 0.1$, the radiative accelerations always are at least 10 times smaller than the gravitational acceleration in the line-forming region, so that helium should indeed diffuse below the photosphere and become underabundant. However, even at the abundances derived here, $N(\mathrm{He})/N(\mathrm{H}) \sim 0.01$, the radiative acceleration remains less than the gravitational acceleration, and diffusion should lead to abundances even lower than are observed. The observed abundances thus cannot be explained simply by the balance between gravitational and radiative accelerations, and other processes must be invoked. Mass loss is one attractive possibility; Michaud et al. (1985) have shown that the equilibrium abundances of heavy elements in sdOB stars can be modified significantly in the presence of a mass-loss rate of only $2 \times 10^{-15}$ $M_\odot$ yr$^{-1}$. Such calculations for helium have not yet been reported. Moreover, such low-mass rates are completely undetectable observationally. The explanation for the observed helium underabundances in classical sdB and sdOB stars thus remains a open question.

J. L. acknowledges support from the National Science Foundation through grant AST 92-17961. P. B. acknowledges support from the NSERC Canada and from the Fund FCAR (Québec). The authors are grateful to S. Moehler and U. Heber for making possible comparisons with previous work, and to R. Green for valuable discussions.

## REFERENCES

Allen, C. W. 1973, Astrophysical Quantities (London: Athlone)
Armandroff, T. E. 1988, AJ, 96, 588
Baschek, B., Höflich, P., & Scholz, M. 1982a, A&A, 112, 76
Baschek, B., Kudritzky, R. P., Scholz, M., & Simon, K. P. 1982b, A&A, 108, 387
Baschek, B., & Norris, J. 1975, ApJ, 199, 694
Bergeron, P., Fontaine, G., Lacombe, P., Wesemael, F., Crawford, D. L., & Jakobsen, A. M. 1984, AJ, 89, 374
Bergeron, P., Saffer, R. A., & Liebert, J. 1992, ApJ, 394, 228
Buonnano, R., Corsi, C. E., & Fusi Pecci, F. 1985, A&A, 145, 97
Buonnano, R., Corsi, C. E., Fusi Pecci, F., Alcaino, G., & Liller, W. 1984, ApJ, 277, 220
Burstein, D., Bertola, F., Buson, L. M., Faber, S. M., & Lauer, T. R. 1988, ApJ, 328, 440
Caloi, V. 1972, A&A, 20, 357
———. 1989, A&A, 221, 27
Cannon, R. D. 1981, in IAU Colloq. 68, Astrophysical Parameters for Globular Clusters, ed. A. G. D. Philip & D. S. Hayes (Schenectady: Davis), 501
Castellani, V., Chieffi, A., & Straniero, O. 1990, ApJS, 74, 463
Ciardullo, R., Jacoby, G. H., Ford, H. C., & Neill, J. D. 1989, ApJ, 339, 53

Crocker, D. A., Rood, R. T., & O'Connell, R. W. 1986, ApJ, 309, L23
———. 1988, ApJ, 332, 236
Da Costa, G. S., Norris, J., & Villumsen, J. V. 1986, ApJ, 308, 743 (DCNV)
Dorman, B., Rood, R. T., & O'Connell, R. W. 1993, ApJ, 419, 596
Downes, R. A. 1986, ApJS, 61, 569
Fillipenko, A. V. 1982, PASP, 94, 715
Fontaine, G., Wesemael, F., Lamontagne, R., Bergeron, P., & Green, R. F. 1987, in IAU. Colloq. 95, The Second Conference on Faint Blue Stars, ed. A. G. D. Philip, D. S. Hayes, & J. W. Liebert (Schenectady: Davis), 615
Giddings, J. R., & Dworetsky, M. M. 1978, MNRAS, 183, 265
Green, R. F., Schmidt, M., & Liebert, J. 1986, ApJS, 61, 305
Greenstein, J. L. 1971, in IAU Symp. 42, White Dwarfs, ed. W. J. Luyten (Dordrecht: Reidel), 46
Greenstein, J. L., & Sargent, A. I. 1974, ApJS, 28, 157
Groth, H. G., Kudritzki, R. P., & Heber, U. 1985, A&A, 152, 107
Heber, U. 1986, A&A, 155, 33
Heber, U., Hunger, K., Jonas, G., & Kudritzky, R. P. 1984, A&A, 130, 119
Heber, U., Kudritzki, R. P., Caloi, V., Castellani, V., Danziger, J., & Gilmozzi, R. 1986, A&A, 162, 171
Heber, U., & Langhans, G. 1986, in New Insights in Astrophysics (ESA SP-263), ed. E. J. Rolfe (Noordwijk: ESA), 279
Horch, E., Demarque, P., & Pinsonneault, M. 1992, ApJ, 388, L53
Hummer, D. G., & Mihalas, D. 1988, ApJ, 331, 794
Hunger, K., Gruschinske, J., Kudritzki, R. P., & Simon, K. P. 1981, A&A, 95, 244
Iben, I., Jr. 1990, ApJ, 353, 215
Iben, I., Jr., & Tutukov, A. V. 1986a, ApJ, 311, 742
———. 1986b, ApJ, 311, 753
Jacoby, G. H. 1989, ApJ, 339, 39
Katuzny, J., Udalski, A. 1992, A&A, 42, 29
Kilkenny, D., Heber, U., & Drilling, J. S. 1987, in IAU Colloq. 95, The Second Conference on Faint Blue Stars, ed. A. G. D. Philip, D. S. Hayes, & J. W. Liebert (Schenectady: Davis), 731
Kudritzki, R. D., & Hummer, D. G. 1990, ARA&A, 20, 303
Lamontagne, R., Wesemael, F., & Fontaine, G. 1987, ApJ, 318, 844
Lamontagne, R., Wesemael, F., Fontaine, G., & Sion, E. M. 1985, ApJ, 299, 496
Lester, J. B., Gray, R. O., & Kurucz, R. L. 1986, ApJS, 61, 509
Liebert, J., Bergeron, P., & Saffer, R. A. 1991, in The Seventh European Workshop on White Dwarfs, ed. G. Vauclair & E. M. Sion (Dordrecht: Kluwer), 409
McCook, G. P., & Sion, E. M. 1987, ApJS, 65, 603
Mendez, R. H. 1987, in IAU Colloq. 95, The Second Conference on Faint Blue Stars, A. G. D. Philip, D. S. Hayes, & J. W. Liebert (Schenectady: Davis), 191
Mendez, R. H., Miguel, C. H., Heber, U., & Kudritzki, R. P. 1986, in IAU Colloq. 87, Hydrogen Deficient Stars and Related Objects, ed K. Hunger, D. Schönberner, & N. Kameswara Rao (Dordrecht: Reidel), 323
Michaud, G., Bergeron, P., Heber, U., & Wesemael, F. 1989, ApJ, 338, 417
Michaud, G., Bergeron, P., Wesemael, F., & Fontaine, G. 1985, ApJ, 299, 741
Moehler, S., Heber, U., & de Boer, K. S. 1990a, A&A, 239, 275 (MHdB)
Moehler, S., Richtler, T., de Boer, K. S., Dettmar, R. J., & Heber, U. 1990b, A&AS, 86, 53
Newell, B., & Graham, J. A. 1976, ApJ, 204, 804
Norris, J. 1981, ApJ, 248, 177
Norris, J., Cottrell, P. L., Freeman, K. C., & Da Costa, G. S. 1981, ApJ, 244, 205
Olson, E. C. 1974, PASP, 86, 80
Paczyński, B. 1971, Acta Astron., 21, 1
Philip, A. G. D., & Newell, E. B. 1975, Dudley Obs. Rept., 9, 161
Press, W. H., Flannery, B. P., Tuekolsky, S. A., & Vetterling, W. T. 1986, in Numerical Recipes (Cambridge: University Press), 523–537
Rich, M., Minniti, D., & Liebert, J. 1993, ApJ, 406, 489
Rood, R. T., & Crocker, D. 1985, in Horizontal Branch and UV-Bright Stars, ed. A. G. D. Philip (Schenectady: Davis), 99
Saffer, R. A. 1991, Ph.D. thesis, Univ. of Arizona
Schönberner, D., & Drilling, J. S. 1984, ApJ, 278, 702
Smith, G. H., & Norris, J. 1982, ApJ, 254, 149
———. 1983, PASP, 95, 635
Strom, S. E., Strom, K. M., Rood, R. T., & Iben, I., Jr. 1970, A&A, 8, 243
Sweigart, A. V. 1987, ApJS, 65, 95
Sweigart, A. V., Greggio, L., & Renzini, A. 1989, ApJS, 69, 911
———. 1990, ApJ, 364, 527
Sweigart, A. V., & Gross, P. G. 1978, ApJS, 36, 405
Tutukov, A. V., & Yungelson, L. R. 1979, Acta Astron., 29, 665
Weidemann, V., & Koester, D. 1984, A&A, 132, 195
Wesemael, F., Auer, L. H., Van Horn, H. M., & Savedoff, M. P. 1980, ApJS, 43, 159
Wesemael, F., Fontaine, G., Bergeron, P., Lamontagne, R., & Green, R. F. 1992, AJ, 104, 203
Wesemael, F., Holberg, J. B., Veillaux, S., Lamontagne, R., & Fontaine, G. 1985, ApJ, 298, 859